Received November 17, 2020, accepted November 25, 2020, date of publication November 30, 2020,
date of current version December 10, 2020.

Digital Object Identifier 10.1109/ACCESS.2020.3041403

Highly Efficient Planar Metasurface Rectenna

MAGED A. ALDHAEEBI[1], (Member, IEEE), AND THAMER S. ALMONEEF[2], (Member, IEEE)
[1]Department of Electronics and Communication Engineering, Hadhramout University, Mukalla 50512-50511, Yemen
[2]Electrical Engineering Department, College of Engineering, Prince Sattam Bin Abdulaziz University, Al-Kharj 11942, Saudi Arabia

Corresponding author: Thamer S. Almoneef (t.almoneef@psau.edu.sa)

This work was supported by the Deputyship for Research and Innovation, Ministry of Education, Saudi Arabia, under Project 785.

ABSTRACT Simplicity and higher DC efficiency are essential factors to be considered to enhance the overall performance of a rectenna system for microwave electromagnetic energy harvesting and Wireless Power Transfer. To that extent, this letter presents a novel and simple design of a rectenna having high radiation to DC efficiency. The proposed planar rectenna system consists of an 8×8 planar metasurface array with a rectification circuit occupying a supercell of 2×2 while the other cells are terminated with the optimal load resistance. On account of its wide input impedance response, the diode is mounted right at the feed of the metasurface cell, avoiding the use of a matching network between the metasurface cell and the diode. The output DC power of the 4 unit cells within the rectified 2×2 supercell was connected in both series and parallel to study the ability of the rectenna to configure the total output current and voltage. The numerical and experimental results show that the proposed metasurface is capable of capturing the incident electromagnetic waves with radiation to dc conversion efficiencies exceeding 80%.

INDEX TERMS Rectifier circuit, rectenna, metasurface, energy harvesting, dc conversion efficiency.

I. INTRODUCTION

Microwave energy harvesting and Wireless Power Transmission (WPT) has received much attention in many applications, such as health care and biomedical systems, sensors, internet of things applications, and wireless communications [1]–[7]. Metamaterials are artificial materials having electromagnetic properties that show a highly sensitive response to dielectric media [8]. Metamaterials can be made by tightly assembling a large number of subwavelength unit cells where each unit cell having certain shape pattern. By changing the subwavelength unit cell shape and size, the media's permeability and permittivity can be tuned to values such that the impedance of the medium is matched to free space resulting in a reflection coefficient that is zero. If in addition a loss in the medium is introduced, a metamaterial absorber can be designed and utilized for energy harvesting/ scavenging. Metasurface (MSs), however; are two-dimensional (2D) metamaterial planar surfaces consisting of few layers with sub-wavelength thickness to provide excellent abilities to achieve a control over the amplitude, phase, and polarization of electromagnetic wave [9]. The use of metasurfaces to develop energy harvesting and WPT systems is of great interest due to the high absorption capabilities of electromagnetic energy that such surfaces can offer [10].

The overall performance of a WPT system is evaluated based on both its capability of collecting incident electromagnetic radiated power and converting it to AC (antenna), and the ability to convert the collected AC power to DC by the (rectifier) [6]. A rectenna can be designed in a single cell [11]–[13] or in an array form [14]–[16] depending on the requirements of the targeted application. Since the amount of the collected power of a single rectenna is relatively low, an aggregate of rectenna elements can be combined to increase the total collected power level. Different from a single rectenna, an array requires a power combining circuit, which can be before the rectification (AC combining) or post rectification (DC combining), to combine and channel the power to a single load. Such combining circuit adds complexity to the design of a rectenna array and it effects the total efficiency of the rectenna array. In addition, a rectenna can be designed in multiport antenna configuration for increasing the collect RF power at the antenna part of the system with the same overall compact size [17]–[22]. The main objective of using the multiport rectenna is for harvesting the ambient RF using dual-Ports [17] or triple-port and multiple ports [20] with single or multiband of frequencies.

Some pervious published work [23]–[26] concentrated on improving the antenna array efficiency by using array

The associate editor coordinating the review of this manuscript and approving it for publication was Diego Masotti.

metasurfaces, having high radiation to AC efficiency reaching up to 97%. However, those studies did not incorporate a rectification circuit to convert the collected AC power to DC, in addition to the use of vias utilizing an additional layer for mounting the resistors where the collected energy is consumed. The work in [8], [9], [27]–[29] combined the collected AC power from each metasurface unit cell prior to rectification and then fed it to a single rectifier circuit. Because the metasurface cells are tightly coupled, the use of an additional layer to host the combining circuit is inevitable. Moreover, the AC combining circuit will add losses and effect the overall frequency bandwidth response.

Other studies in [30]–[34], developed rectenna arrays with DC combining circuits making the collecting surface a planar one, occupying both the collectors and the rectifiers within the same layer. However such rectenna arrays were limited to a total radiation to DC efficiency of lower than 70%.

In this study, a novel design of a rectenna array made of an ensemble of metasurface unit cells for higher radiation to DC efficiency is introduced. The proposed metasurface array has the capability of collecting electromagnetic energy over a wide impedance response, avoiding the use of a matching network which enables incorporating the rectifier and the collector cells within the same planar layer.

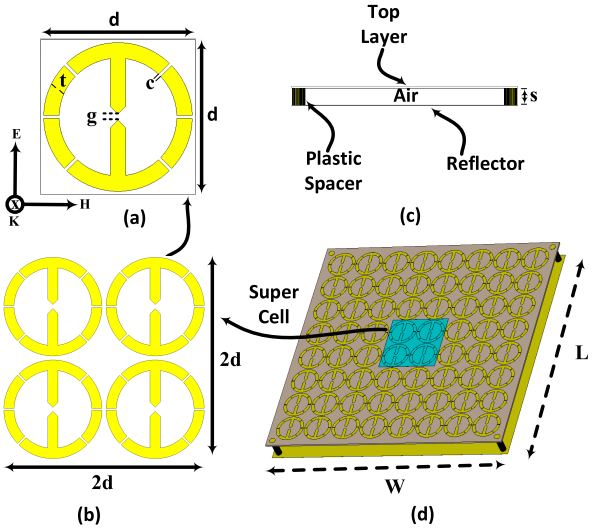

FIGURE 1. Geometry of the proposed planar metasurface showing (a) the unit cell, (b) the supercell consisting of identical 2×2 unit cells, (c) side view of the 8×8 array, and (d) perspective view of 8×8 array.

II. SIMULATION AND DESIGN OF THE UNIT CELL

The single unit cell of the proposed metasurface harvester consists of a loop with an embedded dipole in the middle, a dielectric substrate, an air spacer and a reflector as shown in Fig.1(a). The cell dimensions of the proposed unit cell is designed such that it operates at 2 GHz with $d = 25$ mm, $t = 0.5$ mm and copper thickness $= 35$ μm. The unit cell is designed on top of a Rogers RO4003C dielectric substrate having a $tan\delta = 0.0027$ and a dielectric constant of $\epsilon_r = 3.38$ with a thickness of 1.524 mm. The loop comprises six identical gaps of $c = 0.5$ mm. The electromagnetic energy is received and concentrated within the feed gap of the dipole having a gap length of g $= 0.5$ mm. A terminated variable resistive load is placed across the feed gap to simulate the ability of the metasurface unit cell to receive and consume the collected energy. A ground plane reflector is located at a distance of $S = 15$ mm away from the metasurface as shown in Fig.1(c). The unit cell was simulated using CST Microwave Studio [35]. The proposed supercell consists of identical 2×2 unit cells as shown in Fig.1(b), where the separation between adjacent cells is sep. The dimensions of the proposed dual polarized supercell is designed such that it operates at 2 GHz with a side of $2d = 50$ mm. The purpose of using a supercell is that when using a finite array, the input impedance of the middle unit cells should be similar to the once obtained from the unit cell simulations with periodic boundary condition. However, as we deviate from the middle cells, the input impedance is changed due to the finite array effect. Here, therefore, a supercell is considered so that later in the measurement, the collected energy is tapped from the middle supercell only while all other cells are terminated with optimal load resistances. This is to ensure that the middle supercell experience the required coupling effect from the periodicity of the surrounding cells and the input impedance is as expected from the simulated one. In addition, when using a supercell that contains multiple cells, the output DC power of each subcell can be connected with other subcells in series or parallel to boost either the current or the voltage depending on the type of the connected load.

The S-parameters specifically, the reflection coefficient (S11) and the transmission coefficient (S21) were used to calculate the absorption, reflection, and transmissions of the unit cell. The absorption of the unit cell is obtained by the following equation (1):

$$A = 1 - (S_{11})^2 - (S_{21})^2. \quad (1)$$

Figure2 shows the absorption, reflection, and transmissions of the proposed unit cell as a function of frequency. From the results, it is evident that the unit cell can absorb at least 90% of the incident electromagnetic energy over a wide-band of frequencies from 1.7-4 GHz. Due to the existence of the reflector, the transmission coefficient is zero since all the energy is blocked from leaving the unit cell by the reflector.

In the simulation, first, the distance off between the proposed unit cell and the ground plane reflector was varied from $S = 5$ mm, $S = 10$ mm, $S = 15$ mm, $S = 20$ mm, and $S = 25$ mm (please refer to Fig. 1(c) for the separation distance (S) values of the proposed structure). In all the five cases of varies distance (S), the resistive loads are swept over the range from $R = 100$ Ω to $R = 300$ Ω. Then the efficiency of the unit cell is computed. Numerical results showing the efficiency of the proposed unit cell with various separation values of $S = 5$ mm, to $S = 25$ mm, are presented in Fig. 3. From the results, the efficiency peaks when the unit

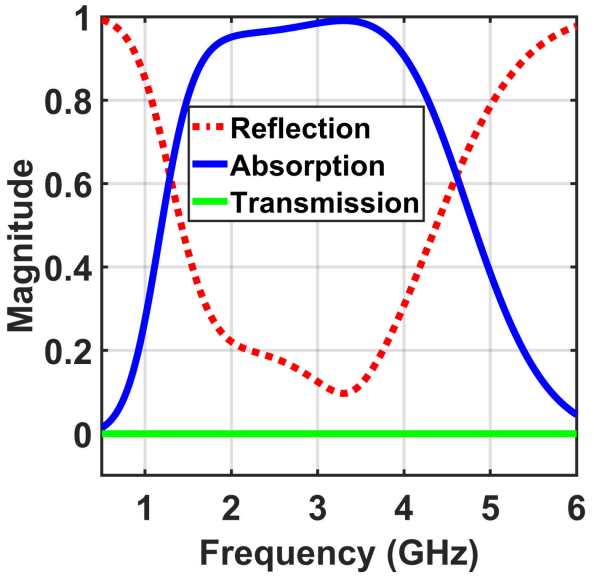

FIGURE 2. Simulation results of the proposed unit cell showing the absorption, reflection and transmission coefficients.

cell is terminated by a load resistance of $R = 150\ \Omega$ and a separation distance (S), between the top layer of the unit cell and the ground plane reflector, of $S = 15\ \Omega$ with maximum efficiency of 98% as shown in Fig. 3 (c). Here, the optimal S value is selected such that it provides the highest efficiency and widest frequency and impedance bandwidth for all the considered load resistances.

In the next simulation setup, the proposed unit cell is carefully studied to ensure that all the dimensions are optimal to produce a surface that maximizes the conversion efficiency. In the simulation study, the unit cell variables of gap g, cuts c and trace width t were varied and the efficiency is analysed for a scan of points. To demonstrate this, a numerical simulation study is carried out with different sizes of the gap varying from $g_1 = 0.15\ mm$ to $g_6 = 1.15\ mm$ with the optimal resistive load of 150 Ω and optimal distance $S = 15\ mm$ between the surface and the reflector. In all six different gap values, the efficiency is recorded over a range of frequencies. Figure 4 shows the numerical results of the efficiency with varies gap values. From the results, we can see that although the highest efficiency can be achieved with a gap size of $g_3 = 0.5\ mm$, the efficiency is not sensitive to varies gap values. However, a slight frequency shift is observed due to the variation in the gap capacitance which results in a shift of the overall resonance frequency of the unit cell.

Next, a numerical simulation is extended to study the effect of different cut sizes on the unit cell's conversion efficiency. The cut values were varied from $c_1 = 0.25\ mm$ to $c_7 = 1.25\ mm$ with a gap value fixed at the optimal obtained value of $g_3 = 0.5\ mm$, optimal resistive load of 150 Ω, and optimal separation of $S = 15\ mm$. In all seven different values of the cuts, the efficiency is recorded over a range of frequencies. Figure. 5 shows the numerical results of the efficiency with varied cuts where the highest efficiency can be achieved at the optimal value of cut size of $c_3 = 0.5\ mm$.

In the next simulation of the proposed unit cell, we investigated the effect of the trace width on the efficiency as a function of frequency of the proposed unit cell and at the optimal obtained values of $c_3 = 0.5\ mm$, $g_3 = 0.5\ mm$, resistive load of 150 Ω, and $S = 15\ mm$. Figure. 6 shows the numerical results of efficiency with varied trace width t from $t_1 = 1\ mm$ to $t_5 = 3.25\ mm$, where the higher efficiency can be achieved at the optimal trace value of $t_4 = 2.5\ mm$. Note here that for all the numerical studies performed above, the conversion efficiency experience negligible effect by the changes of the gap, the cut and the trace width sizes. This is very critical as any tolerances due to fabrication error can lead to a slight frequency shift but without degrading the overall efficiency of the metasurface.

In the last simulation of the proposed unit cell as showing in Fig. 1(a), the unit cell was simulated and updated for the optimal parameters of resistive load of 150 Ω, $S = 15\ mm$, $g_3 = 0.5\ mm$, $c_3 = 0.5\ mm$ and $t_4 = 2.5\ mm$. Figure. 7 shows the numerical results of efficiency with the optimal parameters of the proposed unit cell.

The wide impedance response can be attributed to the six cuts introduced in the proposed unit cell resonator design. To illustrate the effect of the added cut gaps, a simulation study was performed using four scenarios as follows: case (a) the unit cell has only one main gap in the middle of the dipole, case (b) the unit cell has two gaps in addition to the one main gap in the middle of the dipole, (c) the unit cell has four gaps in addition to the one main gap in the middle of the dipole, and (d) the unit cell has six gaps in addition to the main gap in the middle of the dipole as shown in the Fig. 8. We can observe that as the number of cut gaps increases, the electric field is developed and distributed along the introduced gaps equally, creating more degree of freedom of the proposed design. Such increased cut gaps resulted in wider impedance response and frequency response as shown in Fig. 8(d) as compared to Figs. 8 (a), (b) and (c). Such increased number of gaps is analogous to the order number in resonators and filter design where the higher number of elements can result in higher degree of freedom to achieve a wider bandwidth response.

III. SIMULATION AND DESIGN OF 8×8 METASURFACE ABSORBER

The proposed metasurface harvester consists of a periodic array of identical 8×8 unit cells with dimensions as explained above and as shown in Fig. 1(d). The overall array size is L = 210 mm × W=210 mm. In the numerical simulation, all unit cells were terminated by variable resistive loads, placed across the feed gap of each unit cell. The resistive load will next be changed by a diode to measure the DC conversion efficiency of the metasurface and to analyse how the metasurface behaves to various load resistances. The proposed metasurface was simulated in the receiving mode

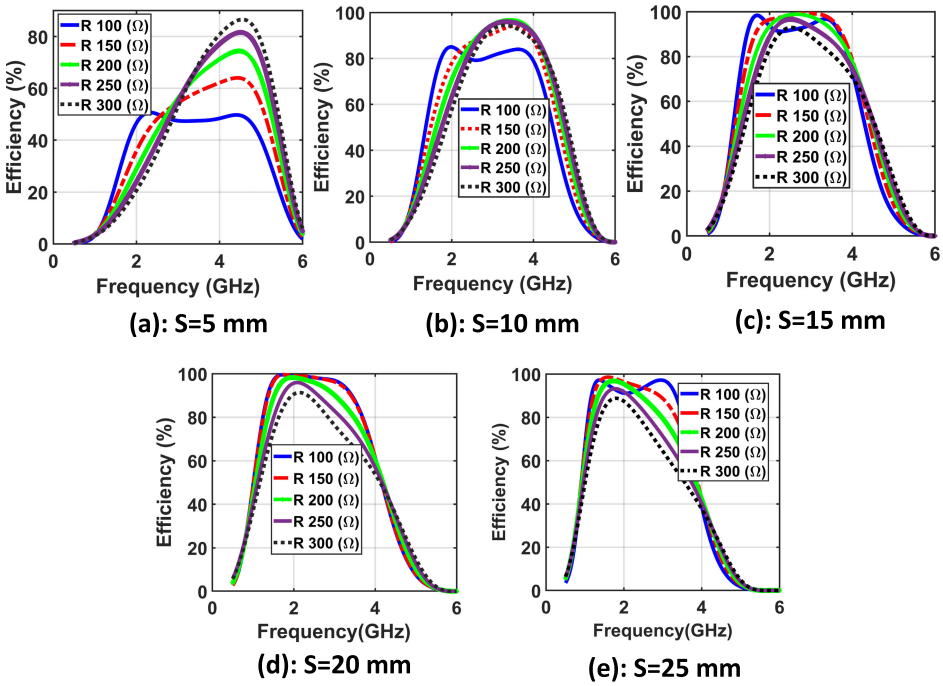

FIGURE 3. Simulation results of the presented unit cell, demonstrating the efficiency with varied resistive loads from 100 Ω to 300 Ω with a separation distance between the top layer and the reflector of: (a) $S = 5$ *mm*, (b) $S = 10$ *mm*, (c) $S = 15$ *mm*,(d) $S = 20$ *mm*, and (e) $S = 25$ *mm*.

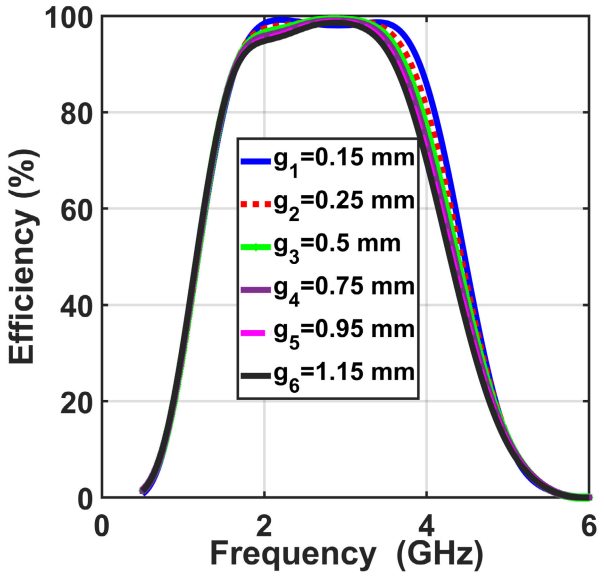

FIGURE 4. Numerical results of the presented unit cell, demonstrating the efficiency with various gap values from $g_1 = 0.15$ *mm* to $g_6 = 1.15$ *mm* with optimum stand off distance between the top layer and reflector of $S = 15$ *mm* and resistive load $R = 150$ Ω.

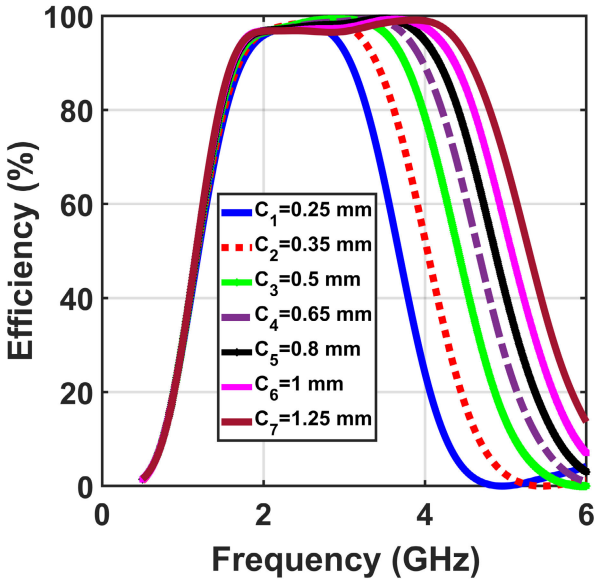

FIGURE 5. Numerical results of the introduced unit cell, demonstrating the efficiency with various cut c values from $c_1 = 0.25$ *mm* to $c_7 = 1.15$ *mm* with optimum stand off distance between the top layer and reflector of $S = 15$ *mm* and resistive load $R = 150$ Ω.

with a planewave excitation having polarization as illustrated in Fig. 1(a). The efficiency of the metasurface is computed by the following equation (2):

$$\eta = \frac{P_d}{P_{in}} \tag{2}$$

where the input power, P_{in}, is the real power available on the footprint of the harvester in Watts. Note here that P_{in} can be obtained by multiplying the footprint area of the metasurface by the poynting vector above the surface of the harvester.

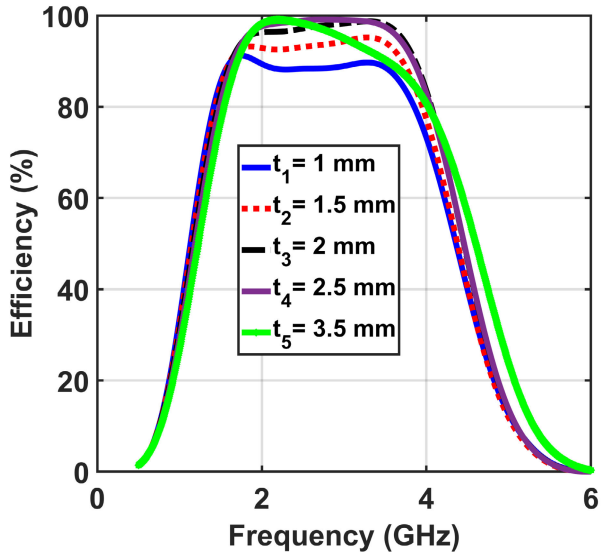

FIGURE 6. Simulation results of the proposed unit cell, demonstrating the efficiency with various trace width t values from $t_1 = 1$ *mm* to $t_5 = 3.25$ *mm* with optimum stand off distance between the top layer and reflector of $S = 15$ *mm* and resistive load $R = 150\ \Omega$.

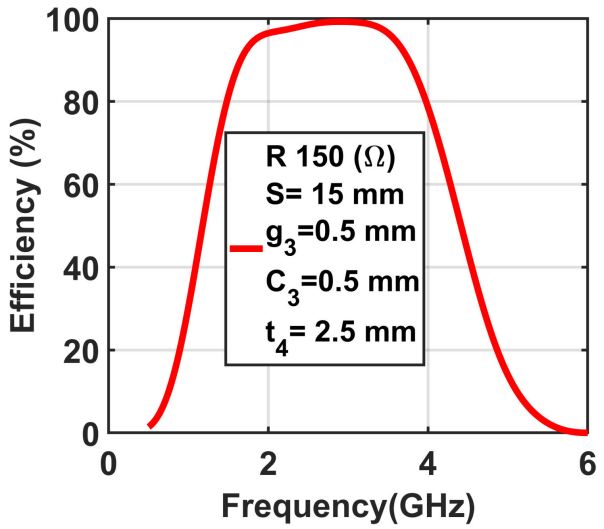

FIGURE 7. Simulation results of the proposed unit cell, demonstrating the efficiency with optimal parameters of resistive load of 150 Ω, $S = 15$ *mm*, $g_3 = 0.5$ *mm*, $c_3 = 0.5$ *mm* and $t_4 = 2.5$ *mm*.

The developed power, P_d, can be calculated by summing all the developed power across all the load resistors of each unit cell. Such power can be either AC or DC depending on the type of harvester and the existence of diodes.

Furthermore, the metasurface has the capability to capture microwave energy with a wide range of terminated load resistances in range from 100 Ω to 300 Ω with efficiencies exceeding 85% as shown in Fig. 9. Because the input impedance of most diodes are within this resistance range, a diode can be mounted right across the metasurface feed gap without a matching network. Thus, the rectenna design can be simplified and the total size of the harvester can be reduced.

Figures 10 and 11 show the magnitude of surface current and the E-field respectively across the surface of the 8×8 metasurface at a frequency of 2 GHz. From the figure, the strength of the surface current and E-field are illustrated across the 8×8 cells by blue color and red color which corresponds to the lowest and highest magnitude, respectively. From the results, it is interesting to note that here both the surface current and electric field variations experience high magnitudes across the gap of the dipole of each unit cells which is the location of the port where the energy is consumed. This is due to the fact that the energy of each unit cell is captured, channeled and confined across the load resistance where the diode will be placed for radiation to DC conversion.

IV. FABRICATION AND MEASUREMENT RESULTS

The developed metasurface is fabricated and measured as shown in Fig. 12. Figure 12(b) shows the 8×8 unit cells hosted on a Rogers RO4003C dielectric substrate. In the fabricated metasurface, the 4 middle cells forming a 2×2 supercell were terminated by a Schottky diode at the feed gap of each subcell. The rest of the surrounding cells were terminated by the optimal resistor load obtained in the simulation, 150 Ω.

In the measurement, the fabricated 8×8 unit cells were terminated at the feed location by either a Schottky diode or a resistor. The middle cells were terminated by an SMS7621 Schottky diodes, while the other 60 surrounding cells were terminated by the optimal resistors as shown in Fig. 13.

Since the metasurface cell has a wide impedance bandwidth response seen from the feed gap point of view, the SMS7621 Skyworks Schottky diode is connected across the feed gap of the cells, avoiding the use of a matching circuitry between the metasurface cell and the diode which in turn minimizes the size of the metasurface in addition to reducing the losses that could have been introduced by the matching network. A pair of 100 *nH* SMT L-14CR10JV4T inductors were placed at the two sides of each diode to filter out the RF signal and pass the DC rectified power, then channel it to the load as illustrated in Fig. 14.

In the experiment, the fabricated rectenna system was positioned a distance of 1 *m* away from a high gain transmitting array antenna. The antenna was connected to a signal generator through a 36 *dB* gain high power amplifier to allow for a wide sweeping range of the input power as shown in Fig. 15.The incident power was carefully obtained by taking the power gain and power loss of all the devices used in the experiment. First the power is generated by a signal generator, then the output power of the generator is amplified by a high power amplifier. The output of the amplifier is then fed to the transmitting log-periodic antenna. Friis's equation was then used to calculate the received power by the metasurface. In addition, all the cables and connectors were characterized, and the losses were considered to calculate the incident power accurately.

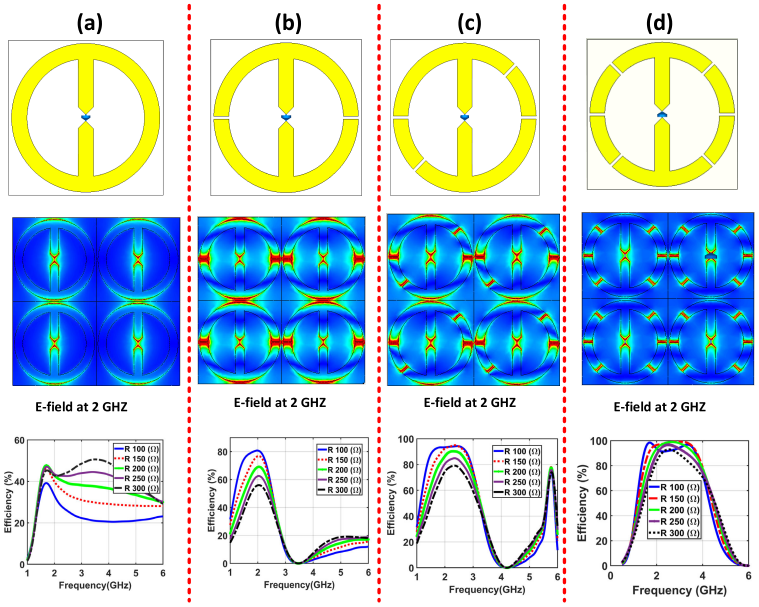

FIGURE 8. Geometry, electric field distribution and simulation results of the efficiency comparing the proposed unit cell with the other three studied cases, demonstrating the novelty of the proposed wide impedance bandwidth unit cell. (a) case a, (b) case b, (c) case c and (d) case d as described within the manuscript.

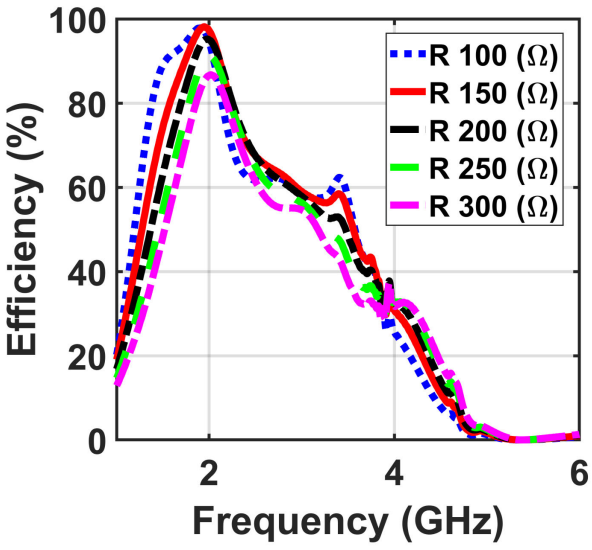

FIGURE 9. Simulation results of the presented metasurface, demonstrating the efficiency with varied resistive loads from 100 Ω to 300 Ω with optimum stand off distance between the top layer and reflector of $S = 15$ *mm*.

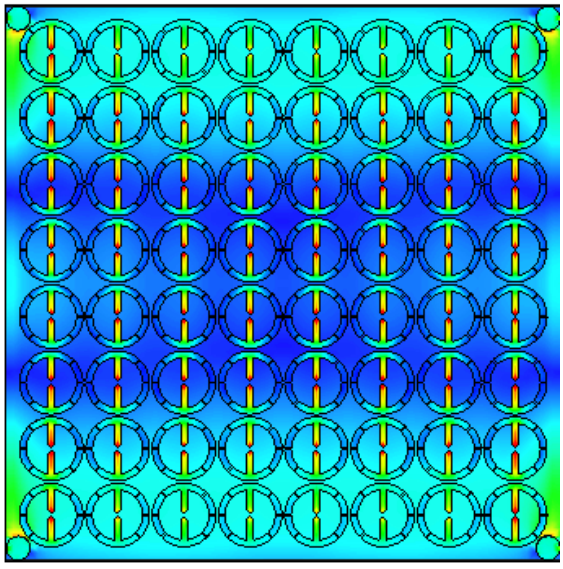

FIGURE 10. Numerical results showing the magnitude of the surface current across the surface of the 8×8 metasurface at a frequency of 2 GHz. From the figure, the blue and red colors corresponds to the lowest and highest magnitude of the surface current, respectively.

In the experimental setup, the DC outputs of the 2×2 supercell were connected in parallel and series to study the possible configurations and the flexibility in varying the total DC current and voltage across the load resistance as outlined in Fig. 9.

To ensure that the harvester is operating at the optimal settings, three different tests were conducted. A resistance sweep was first examined at a fixed frequency and power level for both series and parallel connections as shown in Fig. 16 (a) and (b) for series and parallel connections, respectively. The efficiency peaks at a load resistance of Rs = 1000 Ω for series and Rp = 250 Ω for parallel connection.

The input power level was then varied at the optimal load resistance and frequency as a function of the DC efficiency.

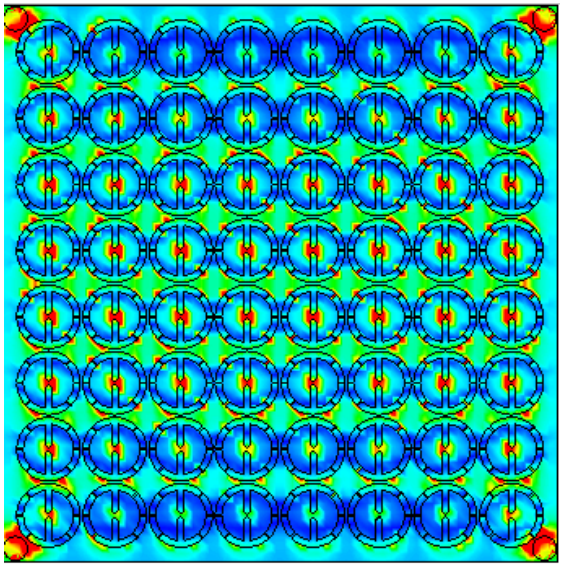

FIGURE 11. Numerical results showing the magnitude of E field across the surface of the 8×8 metasurface at frequency 2 GHz.From the figure, the blue and red colors corresponds to the lowest and highest magnitude of the E-field, respectively.

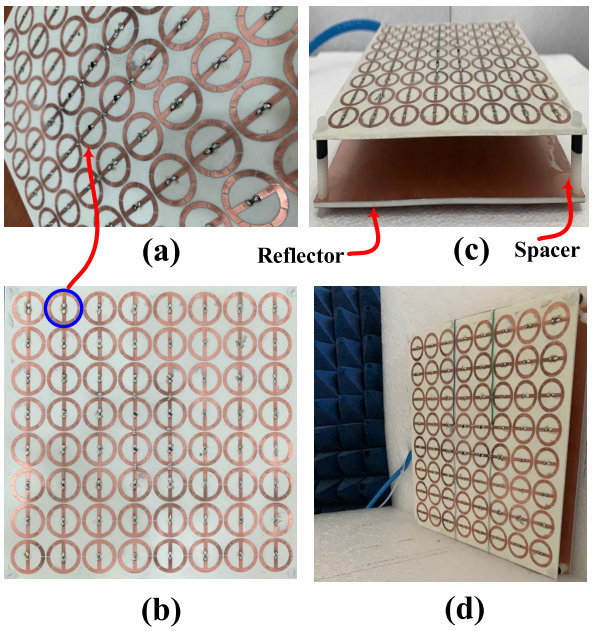

FIGURE 12. A photograph illustrating the fabricated rectenna system: (a) top view, and (b) perspective view.

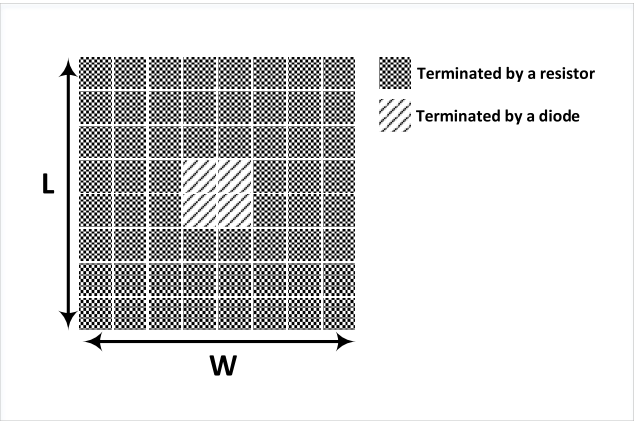

FIGURE 13. schematic illustrating the termination at the feed location of each unit cell by either a Schottky diode or a resistor of the fabricated 8×8 rectenna system.

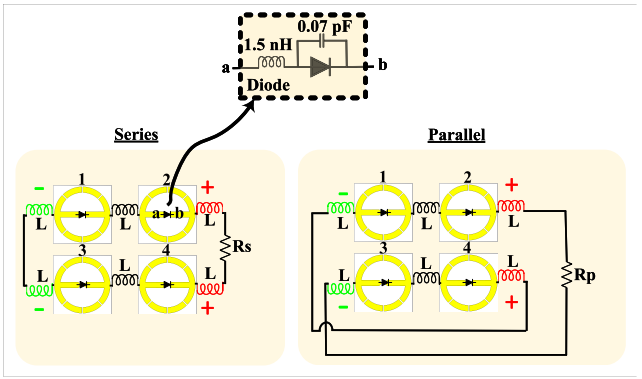

FIGURE 14. A schematic showing an equivalent circuit for the proposed rectenna system when the 2×2 unit cells are combined in (a) series and (b) parallel.

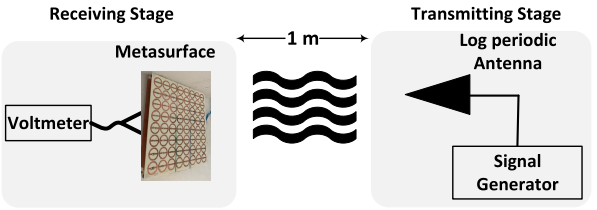

FIGURE 15. Schematic showing experimental setup for measuring the DC power harvesting efficiency of the fabricated rectenna system.

Figure 17 shows experimental results of the DC efficiency as a function of the input power sweep for both parallel and series connections, with radiation to DC efficiency reaching 82% for series and 79% for parallel connections. For both connections, the efficiency is maximum at an optimal power level of -5 *dBm*. Here the power level is calculated by taking the product of the poyinting vector and the footprint area of the harvester under test.

Finally, the experimental test demonstrating the DC efficiency with frequency sweep was performed while fixing the optimal power level and the optimal load resistance for the two cases of the series and parallel connections. Figure 18 shows the experimental results of the DC efficiency as a function of the frequency sweep for both parallel and series connections.

The results in Fig. 18 show that the DC efficiency reached a maximum of 81% when the operating frequency is 1.9 *GHz*. The obtained high radiation to DC efficiency can be attributed to the careful design of the metasurface unit cell having a high

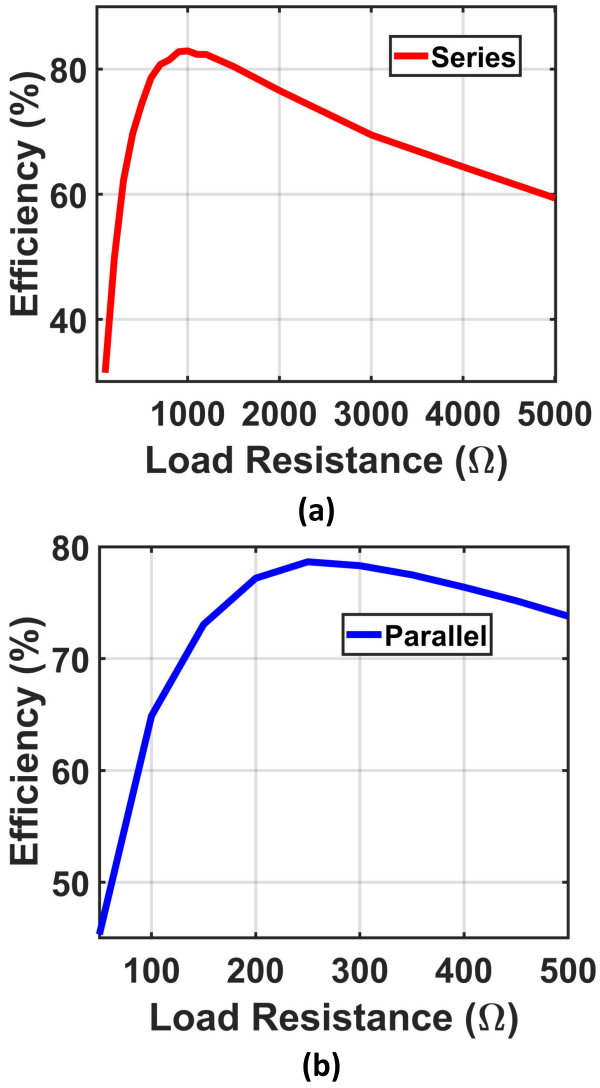

FIGURE 16. Measurement results showing the DC efficiency with different values of load resistance for (a) series and (b) parallel connections.

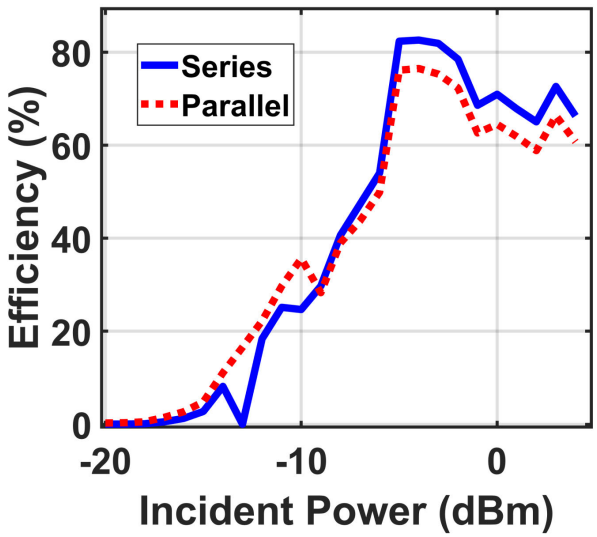

FIGURE 17. Measurement results demonstrating the DC efficiency with the input power sweep for both connection types.

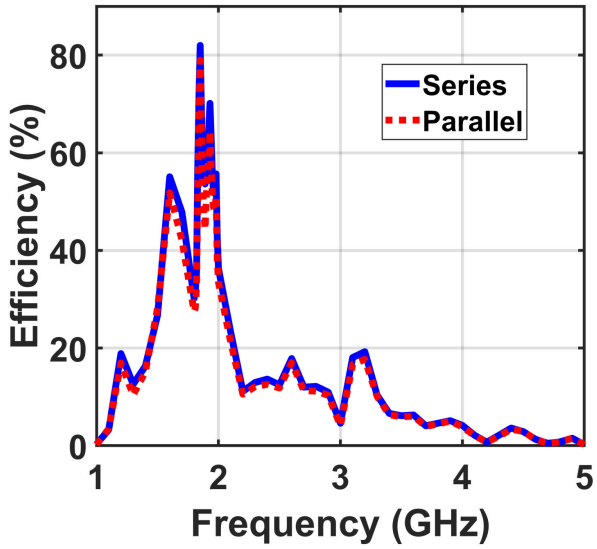

FIGURE 18. Experimental validation of the proposed metasurface showing the radiation to DC efficiency with frequency sweep for both connection types.

absorption efficiency in addition to the wide input impedance response, eliminating any losses associated with a matching network.

To illustrate how the connections among the 4 middle unit cells were performed and the benefit of each connection type, the following analysis is outlined. The proposed super unit cell consisting of 4 sub cells located in the middle of the array were connected in series and parallel as far as the DC power is concerned. From Fig. 9, cells 1 and 2 are connected in series through an RF choke inductor. Similarly, cells 3 and 4 are also connected in series through an inductor and the output of cell combination (1-2) and cell combination (3-4) were connected in series or parallel. At a fixed frequency of 1.85 GHz and input power of -5 dBm and when cell combination (1-2) and (3-4) were connected in series, the obtained measured output voltage was 878 mV and a current of 0.82 mA through an optimal load resistance of 1000 Ω. However, a parallel connection returned a voltage of 419 mV and a current of 1.56 mA through an optimal load resistance of 250 Ω. From the results, we can observe that the current can be doubled when using the parallel connection type as compared to the series one. In the contrary, the voltage can be doubled when using the series connection as compared to the parallel one which is expected from the basic laws of circuit theory and given the fact that we are dealing with DC voltages and currents here due to the use of RF choke inductors before and after the cells, ensuring the flow of only the DC current. Table 1 summarizes the measured results obtained in the experiment for parallel and series connections at a fixed frequency and input power.

TABLE 1. A summary of the measured results obtained in the experiment for parallel and series connections at a fixed frequency and input power.

Connection type	Frequency (GHz)	Voltage (mV)	Current (mA)	Load (Ω)
Parallel	1.85	419	1.56	250
Series	1.85	878	0.82	1000

TABLE 2. A comparative study of the proposed dual polarized rectenna array with various state of the art published Papers.

Reference	Footprint area	Frequency (GHz)	Simplicity - Using Via	Use of matching network	Rad to (AC) or Rad. to (DC)	Efficiency %
[37]	$0.57\lambda \times 0.65\lambda$	5.9	Planar-Yes	No	AC	80%
[26]	$\lambda \times \lambda$	3	Planar-Yes	No	AC	93%
[38]	$0.6\lambda \times 0.6\lambda$	2.45	Planar-Yes	No	AC	97.3%
[27]	$0.9\lambda \times 0.9\lambda$	2.45	Planar-Yes-Dual layer	Yes	DC	67%
[8]	$0.8\lambda \times 0.8\lambda$	2.82	Planar-Yes-Dual layer	Yes	DC	40%
[9]	$1.9\lambda \times 1.9\lambda$	2.72	Planar-Yes-Dual layer	Yes	DC	55%
[29]	$\lambda \times \lambda$	2.45	Planar-Yes-Dual layer	Yes	DC	66.9%
[28]	$0.8\lambda \times 0.8\lambda$	2.4	Planar-Yes-Dual layer	Yes	DC	70%
[32]	$\lambda \times 1.2\lambda$	2.45	Planar-Yes	Yes	DC	44.5%
[31]	$0.3\lambda \times 0.3\lambda$	6.75	Planar-NO	No	DC	50%
[34]	$0.5\lambda \times 0.5\lambda$	2.84	Planar-NO	No	DC	60%
[30]	$0.9\lambda \times 0.8\lambda$	3.4	Planar-NO	No	DC	76%
[33]	$2\lambda \times 2\lambda$	2.1	Planar-NO	No	DC	50%
This work	$0.7\lambda \times 0.7\lambda$	**1.9**	**Planar-NO**	**No**	**DC**	**81%**

To understand the effect of each sub system on the total efficiency, the efficiency of each sub system can be carefully studied and analyzed. The overall efficiency of the rectenna system can be obtained by multiplying the efficiency of the sub systems which are the radiation to AC efficiency due to the electromagnetic collector and the AC to DC efficiency due to the rectifier. Therefore, the overall efficiency can be calculated by:

$$\eta = (\eta_{radtoAC})x(\eta_{ACtoDC}) \tag{3}$$

where the simulated $\eta_{radtoAC}$ is 98% as obtained in Fig. 6. The simulated η_{ACtoDC} can be obtained through the diode model presented in [36]. From the diode model, the efficiency of the rectifier as a function of load resistance at the resonance frequency is shown in Fig. 19. The load resistance of each cell combination used in the experiment is around 500 Ω. This load resistance can be deduced from the tabulated results shown in Table 1. When the cell combinations (1-2) and (3-4) where connected in series the total optimal load resistance was 1000 Ω, which shows that each combination has an optimal resistance of (1000 Ω)÷2 = 500 Ω. This also can be obtained from the parallel combination since the parallel connection resulted in 250 Ω which indicates that each cell combination has an optimal load resistance of 250 Ω × 2 = 500 Ω. From Fig. 19, since the optimal load resistance is 500 Ω, this corresponds to an AC to DC efficiency of 81%. Therefore, the total radiation to DC efficiency at the resonance frequency can be estimated using quation (3) to be $\eta = 0.98 \times 0.81 = 0.80$ *or* 80%. This simulated radiation to DC efficiency agrees well with the one obtained through measurement in Fig. 18.

Table 2 compares the novelty and advantages of the proposed rectenna array introduced in this letter with a number of state of the art rectenna arrays presented in the literature. While the studies in [26], [37], [38] provided high efficiency levels, they did not measure the radiation to DC efficiency and were limited to only radiation to AC efficiency without the use of rectifiers.

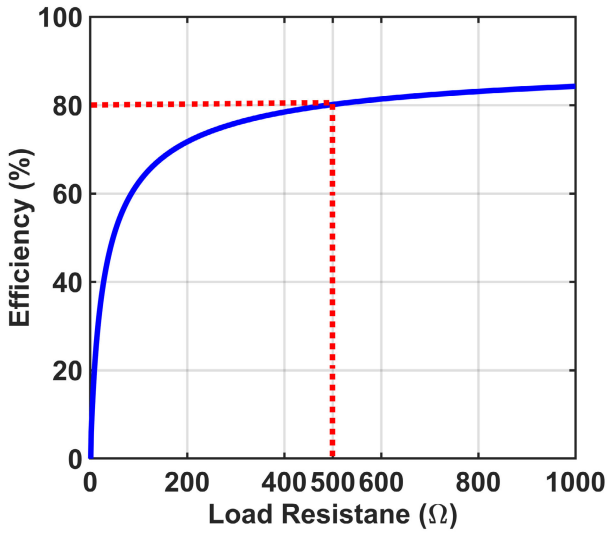

FIGURE 19. Numerical results showing the simulated radiation to DC efficiency.

The introduced studies in [27]–[29] utilize dual layers with vias and matching network between the diode and antenna which adds to the design complexity of the rectenna array compared with the proposed rectenna array in this study.

The developed rectenna array in this work achieves significantly higher DC efficiency (81%) compared with other developed rectenna arrays presented in the literature [30]– [34].

In addition, the proposed design allows for simple connection of tightly placed unit cells where integrating a matching network between the diode and the antenna within the same layer is infeasible due to the limited space between two adjacent cells. Furthermore, the input impedance of the metasurface supercell provided a wide impedance response, enabling the use of diodes right at the feed gap of the cells without the use of matching networks.

V. CONCLUSION

A planer rectenna array design with relatively higher radiation to DC efficiency is presented. The demonstrated planer rectenna array is fabricated in a finite array of 8×8 unit cells where all the cells are terminated with the optimal load resistance of 150 Ω with the exception of the middle supercell of 2×2 that integrates a rectification circuit. The performance of the fabricated planer rectenna array is demonstrated through both simplicity and achieving a higher DC efficiency compared to previously published metasurface arrays. The simplicity of the fabricated planer rectenna array is exhibited by eliminating the use of matching networks due to the wide impedance response of the 2×2 supercell which allows for placing diodes directly at the feed gap of the cells, whereas achieving a higher output efficiency is expressed by measuring the output DC power of the rectified 2×2 supercell in both series and parallel connection, reaching higher than 80% of radiation to DC efficiency.

ACKNOWLEDGMENT

The authors acknowledge the support of the Deanship of Scientific Research at Prince Sattam bin Abdulaziz University, Alkharj, Saudi Arabia.

REFERENCES

[1] Z. Chen, M.-K. Law, P.-I. Mak, and R. P. Martins, "A single-chip solar energy harvesting IC using integrated photodiodes for biomedical implant applications," *IEEE Trans. Biomed. Circuits Syst.*, vol. 11, no. 1, pp. 44–53, Feb. 2017.

[2] M. K. Hosain, A. Z. Kouzani, M. F. Samad, and S. J. Tye, "A miniature energy harvesting rectenna for operating a head-mountable deep brain stimulation device," *IEEE Access*, vol. 3, pp. 223–234, 2015.

[3] C. Zhang, H. Du, and J. Ge, "Energy-efficient power allocation in energy harvesting two-way AF relay systems," *IEEE Access*, vol. 5, pp. 3640–3645, 2017.

[4] K. Shafique, B. A. Khawaja, M. D. Khurram, S. M. Sibtain, Y. Siddiqui, M. Mustaqim, H. T. Chattha, and X. Yang, "Energy harvesting using a low-cost rectenna for Internet of Things (IoT) applications," *IEEE Access*, vol. 6, pp. 30932–30941, 2018.

[5] H. Zhang, Y.-X. Guo, Z. Zhong, and W. Wu, "Cooperative integration of RF energy harvesting and dedicated WPT for wireless sensor networks," *IEEE Microw. Wireless Compon. Lett.*, vol. 29, no. 4, pp. 291–293, Apr. 2019.

[6] Q. Awais, Y. Jin, H. T. Chattha, M. Jamil, H. Qiang, and B. A. Khawaja, "A compact rectenna system with high conversion efficiency for wireless energy harvesting," *IEEE Access*, vol. 6, pp. 35857–35866, 2018.

[7] H. Tafekirt, J. Pelegri-Sebastia, A. Bouajaj, and B. M. Reda, "A sensitive triple-band rectifier for energy harvesting applications," *IEEE Access*, vol. 8, pp. 73659–73664, 2020.

[8] M. El Badawe, T. S. Almoneef, and O. M. Ramahi, "A metasurface for conversion of electromagnetic radiation to DC," *AIP Adv.*, vol. 7, no. 3, Mar. 2017, Art. no. 035112.

[9] M. El Badawe and O. M. Ramahi, "Efficient metasurface rectenna for electromagnetic wireless power transfer and energy harvesting," *Prog. Electromagn. Res.*, vol. 161, pp. 35–40, 2018.

[10] A. A. G. Amer, S. Z. Sapuan, N. Nasimuddin, A. Alphones, and N. B. Zinal, "A comprehensive review of metasurface structures suitable for RF energy harvesting," *IEEE Access*, vol. 8, pp. 76433–76452, 2020.

[11] J. Heikkinen and M. Kivikoski, "A novel dual-frequency circularly polarized rectenna," *IEEE Antennas Wireless Propag. Lett.*, vol. 2, pp. 330–333, 2003.

[12] D. Vital, S. Bhardwaj, and J. L. Volakis, "A 2.45 GHz RF power harvesting system using textile-based single-diode rectennas," in *IEEE MTT-S Int. Microw. Symp. Dig.*, Jun. 2019, pp. 1313–1315.

[13] B. DeLong, A. Kiourti, and J. L. Volakis, "A 2.4-GHz wireless sensor network using single diode rectennas," in *Proc. IEEE Int. Symp. Antennas Propag. (APSURSI)*, Jun. 2016, pp. 403–404.

[14] Y. Yang, J. Li, L. Li, Y. Liu, B. Zhang, H. Zhu, and K. Huang, "A 5.8 GHz circularly polarized rectenna with harmonic suppression and rectenna array for wireless power transfer," *IEEE Antennas Wireless Propag. Lett.*, vol. 17, no. 7, pp. 1276–1280, Jul. 2018.

[15] T. Matsunaga, E. Nishiyama, and I. Toyoda, "5.8-GHz stacked differential rectenna suitable for large-scale rectenna arrays with DC connection," *IEEE Trans. Antennas Propag.*, vol. 63, no. 12, pp. 5944–5949, Dec. 2015.

[16] Y. Ushijima, T. Sakamoto, E. Nishiyama, M. Aikawa, and I. Toyoda, "5.8-GHz integrated differential rectenna unit using both-sided MIC technology with design flexibility," *IEEE Trans. Antennas Propag.*, vol. 61, no. 6, pp. 3357–3360, Jun. 2013.

[17] S. Shen, C.-Y. Chiu, and R. D. Murch, "A dual-port triple-band L-probe microstrip patch rectenna for ambient RF energy harvesting," *IEEE Antennas Wireless Propag. Lett.*, vol. 16, pp. 3071–3074, 2017.

[18] S. Shen, Y. Zhang, C.-Y. Chiu, and R. Murch, "An ambient RF energy harvesting system where the number of antenna ports is dependent on frequency," *IEEE Trans. Microw. Theory Techn.*, vol. 67, no. 9, pp. 3821–3832, Sep. 2019.

[19] H. H. Ibrahim, M. S. J. Singh, S. S. Al-Bawri, and M. T. Islam, "Synthesis, characterization and development of energy harvesting techniques incorporated with antennas: A review study," *Sensors*, vol. 20, no. 10, p. 2772, May 2020.

[20] S. Shen, C.-Y. Chiu, and R. D. Murch, "Multiport pixel rectenna for ambient RF energy harvesting," *IEEE Trans. Antennas Propag.*, vol. 66, no. 2, pp. 644–656, Feb. 2018.
[21] S. K. Divakaran, D. D. Krishna, and Nasimuddin, "RF energy harvesting systems: An overview and design issues," *Int. J. RF Microw. Comput.-Aided Eng.*, vol. 29, no. 1, Jan. 2019, Art. no. e21633.
[22] F. Khalid, W. Saeed, N. Shoaib, M. U. Khan, and H. M. Cheema, "Quad-band 3D rectenna array for ambient RF energy harvesting," *Int. J. Antennas Propag.*, vol. 2020, pp. 1–23, May 2020.
[23] F. Yu, X. Yang, H. Zhong, C. Chu, and S. Gao, "Polarization-insensitive wide-angle-reception metasurface with simplified structure for harvesting electromagnetic energy," *Appl. Phys. Lett.*, vol. 113, no. 12, Sep. 2018, Art. no. 123903.
[24] B. Alavikia, T. S. Almoneef, and O. M. Ramahi, "Wideband resonator arrays for electromagnetic energy harvesting and wireless power transfer," *Appl. Phys. Lett.*, vol. 107, no. 24, Dec. 2015, Art. no. 243902.
[25] B. Ghaderi, V. Nayyeri, M. Soleimani, and O. M. Ramahi, "Pixelated metasurface for dual-band and multi-polarization electromagnetic energy harvesting," *Sci. Rep.*, vol. 8, no. 1, pp. 1–12, Dec. 2018.
[26] T. S. Almoneef and O. M. Ramahi, "Metamaterial electromagnetic energy harvester with near unity efficiency," *Appl. Phys. Lett.*, vol. 106, no. 15, Apr. 2015, Art. no. 153902.
[27] P. Xu, S.-Y. Wang, and W. Geyi, "Design of an effective energy receiving adapter for microwave wireless power transmission application," *AIP Adv.*, vol. 6, Oct. 2016, Art. no. 105010.
[28] T. S. Almoneef, F. Erkmen, and O. M. Ramahi, "Harvesting the energy of multi-polarized electromagnetic waves," *Sci. Rep.*, vol. 7, no. 1, pp. 1–14, Dec. 2017.
[29] X. Duan, X. Chen, and L. Zhou, "A metamaterial electromagnetic energy rectifying surface with high harvesting efficiency," *AIP Adv.*, vol. 6, no. 12, Dec. 2016, Art. no. 125020.
[30] A. Z. Ashoor, T. S. Almoneef, and O. M. Ramahi, "A planar dipole array surface for electromagnetic energy harvesting and wireless power transfer," *IEEE Trans. Microw. Theory Techn.*, vol. 66, no. 3, pp. 1553–1560, Mar. 2018.
[31] G. T. Oumbé Tékam, V. Ginis, J. Danckaert, and P. Tassin, "Designing an efficient rectifying cut-wire metasurface for electromagnetic energy harvesting," *Appl. Phys. Lett.*, vol. 110, no. 8, Feb. 2017, Art. no. 083901.
[32] X. Duan, X. Chen, and L. Zhou, "A metamaterial harvester with integrated rectifying functionality," in *Proc. IEEE/ACES Int. Conf. Wireless Inf. Technol. Syst. (ICWITS) Appl. Comput. Electromagn. (ACES)*, Mar. 2016, pp. 1–2.
[33] T. S. Almoneef, "Design of a rectenna array without a matching network," *IEEE Access*, vol. 8, pp. 109071–109079, 2020.
[34] T. S. Almoneef, F. Erkmen, M. A. Alotaibi, and O. M. Ramahi, "A new approach to microwave rectennas using tightly coupled antennas," *IEEE Trans. Antennas Propag.*, vol. 66, no. 4, pp. 1714–1724, Apr. 2018.
[35] CST. (Sep. 2017). *Computer Simulation Technology. CST Computer Simulation Technology Online*. [Online]. Available: http://www.CST.com
[36] J. O. McSpadden, L. Fan, and K. Chang, "Design and experiments of a high-conversion-efficiency 5.8-GHz rectenna," *IEEE Trans. Microw. Theory Techn.*, vol. 46, no. 12, pp. 2053–2060, 1998.
[37] F. Yu, X. Yang, H. Zhong, C. Chu, and S. Gao, "Polarization-insensitive wide-angle-reception metasurface with simplified structure for harvesting electromagnetic energy," *Appl. Phys. Lett.*, vol. 113, no. 12, Sep. 2018, Art. no. 123903.
[38] X. Duan, X. Chen, Y. Zhou, L. Zhou, and S. Hao, "Wideband metamaterial electromagnetic energy harvester with high capture efficiency and wide incident angle," *IEEE Antennas Wireless Propag. Lett.*, vol. 17, no. 9, pp. 1617–1621, Sep. 2018.

MAGED A. ALDHAEEBI (Member, IEEE) was born in Hadhramout, Yemen, in 1983. He received the B.S. degree in electrical engineering from Hadhramout University, Al Mukalla, Yemen, in 2009, the M.Sc. degree in electrical engineering from King Saud University, Riyadh, in 2014, and the Ph.D. degree from the University of Waterloo, Waterloo, ON, Canada, in 2020. His research interests include energy harvesting, metasurface design, sensor design, and microwaves near-field detection modalities.

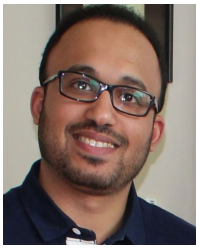

THAMER S. ALMONEEF (Member, IEEE) received the B.S. degree in electrical and computer engineering from Dalhousie University, Halifax, NS, Canada, in 2009, and the M.A.Sc. and Ph.D. degrees in electrical and computer engineering from the University of Waterloo, Waterloo, ON, Canada, in 2012 and 2017, respectively. In 2012, he was appointed as a Lecturer and was granted a scholarship from Prince Sattam Bin Abdulaziz University, Saudi Arabia, to pursue his Ph.D. degree studies. He is currently an Assistant Professor with the Department of Electrical and Computer Engineering, Prince Sattam University, Alkarj, Saudi Arabia. He has authored or coauthored more than 35 refereed journals and conference papers. His research interests include antenna theory, metamaterials and its wide range applications, metamaterial absorbers, electrically small resonators, rectennas, microwave sensors and imagers, electromagnetic energy harvesting, and renewable energy.